Applied Mathematics & Information Sciences
An International Journal

http://dx.doi.org/10.18576/amis/200615

Finite Element Analysis of a Coupled GN-III Thermoelastic Semiconductor Model Under Temperature-Dependent Conductivity

Eman Al-Lehaibi[1], *Ibrahim Abbas*[2,*] *and Aatef Hobiny*[3]

[1] Mathematics Department, Jamoum University College, Umm Al-Qura University, Jamoum 25375, Saudi Arabia
[2] Mathematics Department, Faculty of Science, Sohag University, Sohag, Egypt
[3] Department of Mathematics, Faculty of Science, King Abdulaziz University, Jeddah, Saudi Arabia

Received: 27 Jul. 2026, Revised: 2 Sep. 2026, Accepted: 3 Oct. 2026
Published online: 1 Nov. 2026

Abstract: This study examines the effect of temperature-dependent thermal conductivity on the coupled thermomechanical behavior of a semiconductor medium within the fully coupled Green–Naghdi type III theory. The governing thermal, elastic, and carrier-density equations are solved numerically using the finite element method under an exponentially decaying surface heat flux. The results demonstrate that variable thermal conductivity significantly affects the magnitudes and propagation of all coupled fields. The numerical formulation is validated against published analytical solutions for the constant-conductivity limit, showing excellent agreement. The proposed model provides a reliable framework for analyzing coupled thermoelastic processes in semiconductors with temperature-dependent thermal properties.

Keywords: Varying thermal conductivity; finite element scheme; fully coupled Green–Naghdi (GNIII) model.

Nomenclature

Symbol	Description
E_g	Semiconductor energy gap
K_0	Conductivity rate parameter
t_0	Heat flux pulse time
α_T	Thermal expansion coefficient
K	Thermal conductivity
u_i	Components of displacement
e	Particle charge
D_e	Carrier diffusion coefficient
σ	Electric conductivity
N_0	Carrier density equilibrium
C_e	Specific heat
d_n	Electronic deformation coefficient
N	Carrier density
τ	Lifetime
ρ	Density of material
λ, μ	Lamé's constants
σ_{ij}	Components of Stress
E_F	Electro-chemical potential
T_0	Initial temperature
q_0	Constant heating flux

1 Introduction

Due to their relevance to modern engineering applications, particularly in micro and nano devices where the thermal fields, carrier transport, and elastic deformation are coupled, the photothermal and photo-thermoelastic interactions in semiconductor materials are extensively studied. The interactions are more pronounced when advanced thermoelastic theories are used (e.g., generalized theories in which the thermal wave speeds are finite) and when the thermally conductive materials are of variable conductivity within and/or across the gradient, which profoundly impact the response to the fields of temperature, stress, and displacement. Within this context, several studies have addressed semiconductor half-space problems under different theoretical frameworks and boundary excitations.

For decades, thermoelasticity, especially Biot's [1] who integrated some aspects of irreversible thermodynamics, and thermoelasticity, has drawn attention. While Biot was the first to discuss the coupling

* Corresponding author e-mail: ibrabbas7@science.sohag.edu.eg

© 2026 NSP
Natural Sciences Publishing Cor.

of thermodynamics and thermoelasticity, stating that, to some extent, all irreversible thermodynamics are dissipated as heat during the process, and, therefore, the theory of thermodynamic heat is coupled with the theory of elastic heat, it was he who first proposed the theory as irreversible. Subsequently, in the first of a series of remarkable contributions to the theory of thermoelasticity and thermodynamics, Cattaneo [2] proposed a theory where the paradox of instantaneous heat propagation was, to some extent, addressed in the theory of thermodynamics as the heat of a moving medium and the Fourier's law of thermodynamics dissipative flow. Subsequently, of all proposed theories, the one enunciated by Lord and Shulman [3] was the most generalized, for it proposed the theory of thermodynamics with one relaxation time, as Shulman himself proposed. Furthermore, of the many proposed theories, that of Green and Lindsay [4], in the development of a theory of heat transfer rate and temperature, has been the most utilized. Also, the most utilized, as it was introduced in the examination of high velocity thermal phenomena in semiconductors, was that of Green and Naghdi [5, 6].

Earlier work by Todorović and co-authors provided both theoretical formulations and experimental investigations of micromechanical structures, with particular emphasis on the coupled thermoelastic response and associated plasma-field effects [7, 8, 9]. Hobiny and Abbas developed a generalized model (GN) to examine photothermal interaction in a 2D semiconductor half-space, providing analytical insight into coupled responses under generalized thermoelasticity assumptions [10]. Abbas, Hobiny, and Marin further extended photothermal modeling by considering semiconducting media containing cylindrical cavities and incorporating varying thermal conductivity, demonstrating the influence of geometric discontinuities and conductivity variation on the resulting physical fields [11]. Alzahrani et al. investigated photo-thermoelastic interaction in a semiconducting half-space under a formulation that neglects energy dissipation, highlighting the role of generalized theories in capturing wave-like thermal responses [12]. In addition, Alzahrani investigated the impact of varying thermal conductivity in semiconductor material, emphasizing that conductivity variation can substantially modify transient thermal and mechanical behavior [13].

Various other heating profiles and physical phenomena have been studied. Ailawalia and Kumar have studied ramp-type heating in semiconductors from the viewpoint of the photothermoelastic model and illustrated the effects of non-instantaneous thermal loading on the evolution of the coupled fields [14]. Lotfy et al. investigated the combined effect of electromagnetic and Thomson effects, along with thermal memory, in semiconductors subjected to laser pulses during photothermal excitation which shows the growing interest in multi-physics and non-classical heat transport phenomena [15]. Mohamed et al. studied the absorption of illumination in a two-dimensional rotator thermoelastic material under the modified Green–Lindsay theory and reaffirmed the validity of generalized thermoelastic theory for the description of wave propagation in the medium with non-uniform temperature [16]. Outside of semiconductors, similar thermo-mechanical and heat transfer studies further exemplify the utility of considering temperature dependence or variability in thermal conductivities. For instance, Yang et al. have studied numerically the displacement behavior in energy piles under thermo-mechanical loading and highlighted the sensitivity of deformation to coupled thermal interactions in engineering constructions [17]. Khoukhi et al. studied transient temperature changes in insulated walls with variable thermal conductivity, confirming that conductivity variation significantly influences thermal diffusion behavior in building materials [18]. Similarly, Ghasemi et al. analyzed convective fins with temperature-dependent thermal conductivity and internal heat generation, showing how property variation affects thermal performance and temperature distribution [19]. Collectively, these contributions highlight the necessity of incorporating variable thermal conductivity and generalized thermoelastic effects to obtain realistic predictions for photothermal responses in semiconductor and related media. Khamis et al. [20] studied the impact of spatially/temperature-dependent thermal conductivity of semiconductor materials under photothermal excitation focusing specifically on ramp-type thermal loading. More recent contributions [21, 22, 23, 24, 25] have studied phenomena coupled with the photo-thermo-piezoelastic wave propagation, use of fractional-order theory, and memory-dependent heat conduction in semiconducting medium and their impact on the vibrational response and heat conduction in semiconductors within different generalized thermoelastic frameworks. Within this line of research, Sherief et al. [26] developed a formulation for a fully coupled generalized thermoelastic system in semiconductors. His theory addressed the thermal, mechanical and diffusive field coupling, thus extending the theory on how a semiconductor responds to complex loading. More recently, Abbas et al. [27] developed a new photo-thermoelastic wave framework for semiconducting materials based on the Green–Naghdi type III (GNIII) theory of finite thermal wave propagation which incorporates strong thermo-mechanical coupling and does not assume classical diffusion. Numerous authors [28, 29, 30, 31, 32, 33, 34, 35, 36, 37, 38, 39, 40, 41, 42, 43, 44, 45, 46, 47, 48, 49] have employed generalized thermoelasticity formulations to obtain analytical and numerical solutions for a broad class of thermo-mechanical problems under various boundary and loading conditions. An investigation into a new photothermal model in semiconductor materials without energy dissipation was given by Abbas et al. [50]. An investigation by Sherief et al. [51] was conducted Impact of surface recombination velocity on the solid sphere

© 2026 NSP
Natural Sciences Publishing Cor.

issue of two-dimensional thermoelastic semiconductor design.

This paper examines how thermal conductivity variability affects wave propagation in semiconductor materials under the fully coupled Green–Naghdi (GNIII) model. The finite element approach has been used to get the solutions to field equations. Numerical results for all variables are obtained and presented graphically. The numerical solutions have been compared with the previously obtained analytical solutions, ignoring the new parameters, to verify the proposed method.

2 Basic equations

The governing formulations for a fully coupled generalized photothermoelastic model in a semiconductor isotropic material, as derived in [27], describe the mutual interactions among the thermal, elastic, and electronic carrier fields. In the present formulation, the effects of carrier generation source, heat source, body forces, are neglected, thereby restricting the analysis to intrinsic material coupling mechanisms and simplifying the resulting model.

2.1 Motion

$$\mu u_{i,jj} + (\mu+\lambda)u_{j,ij} - \beta_t T_{,i} - \beta_n n_{,i} = \rho \frac{\partial^2 u_i}{\partial t^2} \tag{1}$$

2.2 Particle diffusion equation

$$D_n\left(b\nabla^2 n - \beta_n \nabla^2 u_{k,k} + a\nabla^2 T\right) = \frac{n-n_o}{\tau} + \frac{\partial n}{\partial t} \tag{2}$$

2.3 Heat conduction formulation

$$\left(k^*(T)T_{,i} + k(T)\frac{\partial T_{,i}}{\partial t}\right)_{,i} = \rho c_e \frac{\partial^2 T}{\partial t^2} + \beta_t T_o \frac{\partial^2 u_{i,i}}{\partial t^2} - \frac{E_g}{\tau}\frac{\partial n}{\partial t} \tag{3}$$

2.4 Constitutive equations

$$\sigma_{ij} = \mu(u_{j,i} + u_{i,j}) + \left(\lambda u_{k,k} - \beta_t(T-T_o) - \beta_n(n-n_o)\right)\delta_{ij} \tag{4}$$

$$M = b(n-n_o) - \beta_n u_{k,k} + a(T-T_o) \tag{5}$$

where $b = \frac{D_e q_o^2}{\sigma_o}$, $D_n = \frac{\sigma_o}{q_o^2}$, $a = \frac{E_g}{T_o}$, $\beta_n = (2\mu+3\lambda)\alpha_n$, $\beta_t = (2\mu+3\lambda)\alpha_t$, and $j,i,k = 1,2,3$.

Where k and k^* are assumed to be temperature dependent as represented in [52]:

$$k(T) = k_o e^{\alpha(T-T_o)}, \quad k^*(T) = k_o^* e^{\alpha(T-T_o)} \tag{6}$$

where α is the negative parameter and k_o, k_o^* are the thermal conductive and conductivity rate parameter when $T = T_o$, respectively.

Let us assume an isotropic unbounded semiconductor material $x \geq 0$. The equations (1)–(5) can be represented with respect to the state of the medium, which is a function of the spatial variable x and the temporal variable t, so we have:

$$(\lambda+2\mu)\frac{\partial^2 u}{\partial x^2} - \beta_t \frac{\partial \theta}{\partial x} - \beta_n \frac{\partial N}{\partial x} = \rho \frac{\partial^2 u}{\partial t^2} \tag{7}$$

$$D_n\left(b\frac{\partial^2 N}{\partial x^2} - \beta_n \frac{\partial^3 u}{\partial x^3} + a\frac{\partial^2 \theta}{\partial x^2}\right) = \frac{\partial N}{\partial t} + \frac{N}{\tau} \tag{8}$$

$$\frac{\partial}{\partial x}\left(k_o^* e^{\alpha\theta}\frac{\partial \theta}{\partial x} + k_o e^{\alpha\theta}\frac{\partial^2 \theta}{\partial t \partial x}\right) = \rho c_e \frac{\partial^2 \theta}{\partial t^2} - \frac{E_g}{\tau}\frac{\partial N}{\partial t} + \beta_t T_o \frac{\partial^3 u}{\partial t^3 \partial x} \tag{9}$$

$$\sigma_{xx} = (\lambda+2\mu)\frac{\partial u}{\partial x} - \beta_n N - \beta_t \theta \tag{10}$$

$$M = bN - \beta_n \frac{\partial u}{\partial x} + a\theta \tag{11}$$

where u represents the x-direction displacement component, $N = n - n_o$ is the carrier density changing and $\theta = T - T_o$ is the temperature increment.

Initial and boundary conditions

The initial and boundary conditions are expressed by

$$u(x,0) = 0, \quad \theta(x,0) = 0, \quad N(x,0) = 0, \quad \frac{\partial u(x,0)}{\partial t} = 0, \quad \frac{\partial N(x,0)}{\partial t} = 0, \quad \frac{\partial \theta(x,0)}{\partial t} = 0 \tag{12}$$

$$N(0,t) = 0, \quad \sigma_{xx}(0,t) = 0, \quad k\frac{\partial \theta(0,t)}{\partial x} = -Q_o \frac{t^2 e^{-\frac{t}{t_p}}}{16 t_p^2} \tag{13}$$

For consistency and proper scaling, the dimensionless parameters may be written as follows.

$$\theta' = \frac{\theta}{T_o}, N' = \frac{N}{n_o}, k_1' = T_o k_1, (\tau', t', t_p') = c^2\eta(\tau, t, t_p), \quad M' = \frac{M}{n_o b}, (u', x') = \eta c(u, x), \sigma_{xx}' = \frac{\sigma_{xx}}{\lambda+2\mu} \tag{14}$$

© 2026 NSP
Natural Sciences Publishing Cor.

where $\eta = \frac{\rho c_e}{k}$ and $c^2 = \frac{\lambda+2\mu}{\rho}$. Using the dimensionless variables described in (14), the governing equations can be expressed as.

$$\frac{\partial^2 u}{\partial x^2} - f_1 \frac{\partial N}{\partial x} - f_2 \frac{\partial \theta}{\partial x} = \frac{\partial^2 u}{\partial t^2} \tag{15}$$

$$\frac{\partial^2 N}{\partial x^2} - f_3 \frac{\partial^3 u}{\partial x^3} + f_4 \frac{\partial^2 \theta}{\partial x^2} = f_5 \left(\frac{N}{\tau} + \frac{\partial N}{\partial t} \right) \tag{16}$$

$$e^{\alpha\theta} \left(f_6 \frac{\partial^2 \theta}{\partial x^2} + \frac{\partial^3 \theta}{\partial t \partial x^2} \right) + \alpha e^{\alpha\theta} \left(f_6 \left(\frac{\partial \theta}{\partial x} \right)^2 + \frac{\partial \theta}{\partial x} \frac{\partial^2 \theta}{\partial t \partial x} \right) = \frac{\partial^2 \theta}{\partial t^2} - \frac{f_7}{\tau} \frac{\partial N}{\partial t} + f_8 \frac{\partial^3 u}{\partial t^2 \partial x} \tag{17}$$

$$\sigma_{xx} = \frac{\partial u}{\partial x} - f_1 N - f_2 \theta \tag{18}$$

$$M = N - f_3 \frac{\partial u}{\partial x} + f_4 \theta \tag{19}$$

where $f_1 = \frac{\beta_n n_o}{\lambda+2\mu}$, $f_2 = \frac{\beta_t T_o}{\lambda+2\mu}$, $f_3 = \frac{\beta_n}{n_o b}$, $f_4 = \frac{T_o a}{n_o b}$, $f_5 = \frac{1}{b\eta D_n}$, $f_6 = \frac{k^*}{\rho c_e c^2}$, $f_7 = \frac{E_g n_o}{T_o \rho c_e}$, $f_8 = \frac{\beta_t}{\rho c_e}$.

3 Finite element approach

The coupled governing relations derived in the previous section constitute a system of nonlinear partial differential equations. To obtain reliable numerical solutions, the finite element method (FEM) is adopted, following the standard weak-formulation framework reported in [53, 54, 55, 56, 57, 58, 59]. The dimensionless weak forms of the governing equations are constructed by introducing admissible test functions associated with the carrier density, temperature, and displacement, denoted by δN, $\delta\theta$, and δu, respectively. Each governing equation is multiplied by its corresponding test function and integrated over the spatial domain, while the boundary conditions are incorporated through the resulting boundary (natural) terms. Within each element, the primary unknown fields are approximated by standard interpolation (shape) functions. Accordingly, the temperature θ, carrier density N, and displacement u are expanded in terms of nodal values as

$$\theta(x,t) = \sum_{j=1}^{m} M_j(x)\theta_j(t), \quad N(x,t) = \sum_{j=1}^{m} M_j(x) N_j(t), \quad u(x,t) = \sum_{j=1}^{m} M_j(x) u_j(t) \tag{20}$$

where m is the number of nodes per element and M_j denotes the element shape functions. In the Galerkin formulation, the same functions are used to represent the test (weighting) functions, yielding

$$\delta\theta = \sum_{j=1}^{m} M_j(x)\delta\theta_j, \quad \delta N = \sum_{j=1}^{m} M_j(x)\delta N_j, \quad \delta u = \sum_{j=1}^{m} M_j(x)\delta u_j \tag{21}$$

Time derivatives of the nodal unknowns are subsequently evaluated using an implicit time-integration scheme, which is particularly suitable for the stiffness introduced by coupling and relaxation terms. Using these approximations, the weak (variational) statements corresponding to Eqs. (14)–(16) can be written in the general form

$$\int_0^L \frac{\partial \delta u}{\partial x} \left(\frac{\partial u}{\partial x} - f_1 N - f_2 \theta \right) dx + \int_0^L \delta u \frac{\partial^2 u}{\partial t^2} dx = \left[\delta u \left(\frac{\partial u}{\partial x} - f_1 N - f_2 \theta \right) \right]_0^L \tag{22}$$

$$\int_0^L \frac{\partial \delta N}{\partial x} \frac{\partial M}{\partial x} dx + \int_0^L \delta N \left(f_5 \left(\frac{N}{\tau} + \frac{\partial N}{\partial t} \right) \right) dx = \left[\delta N \frac{\partial M}{\partial x} \right]_0^L \tag{23}$$

$$\int_0^L \frac{\partial \delta\theta}{\partial x} \left(e^{\alpha\theta} \left(f_6 \frac{\partial \theta}{\partial x} + \frac{\partial^2 \theta}{\partial t \partial x} \right) \right) dx + \int_0^L \delta\theta \left(\frac{\partial^2 \theta}{\partial t^2} - \frac{f_7}{\tau} \frac{\partial N}{\partial t} + f_8 \frac{\partial^3 u}{\partial t^2 \partial x} \right) dx = \left[\delta\theta \left(e^{\alpha\theta} \left(f_6 \frac{\partial \theta}{\partial x} + \frac{\partial^2 \theta}{\partial t \partial x} \right) \right) \right]_0^L \tag{24}$$

These variational expressions form the basis for assembling the global finite element system. After spatial discretization and temporal integration, the procedure yields a coupled nonlinear algebraic system in terms of the nodal unknowns $\{u_j, N_j, \theta_j\}$, which can be solved iteratively at each time level.

4 Numerical Results

The sections prior contained various theoretical results, which we will support here with relevant numerical values for the physical constants. This shows that what is purely theoretical is relevant in a practical situation. In

© 2026 NSP
Natural Sciences Publishing Cor.

this context, the physical characteristics of an isotropic semiconductor will be analyzed using silicon as a case study. Considering silicon is a semiconductor with wide-ranging usages, and its electrical and thermal characteristics have been analyzed in detail, it serves as an ideal example [60]:

$$\rho = 2330\,(\mathrm{kg})(\mathrm{m}^{-3}),\ \lambda = 3.64\times10^{10}\,(\mathrm{N})(\mathrm{m}^{-2}),$$
$$\alpha_t = 3\times10^{-6}(\mathrm{k}^{-1}),\ T_o = 300(\mathrm{k}),$$
$$\mu = 5.46\times10^{10}\,(\mathrm{N})(\mathrm{m}^{-2}),\ c_e = 695\,(\mathrm{J})(\mathrm{kg}^{-1})(\mathrm{k}^{-1}),$$
$$\alpha_n = -9\times10^{-31}(\mathrm{m}^3),\ t = 0.5,$$
$$n_o = 10^{20}(\mathrm{m}^{-3}),\ E_g = 1.12\,(\mathrm{eV}),\ q_o = 1.6\times10^{-19}(\mathrm{C}),$$
$$\sigma_o = 1.56\times10^{-3}(\mathrm{s})(\mathrm{m}^{-1}),$$
$$D_e = 2.5\times10^{-3}(\mathrm{m}^2)(\mathrm{s}^{-1}),\ \tau = 5\times10^{-5}(\mathrm{s}),\ Q_o = 200,$$
$$t_p = 0.3.$$

The use of numerical methods provides insight into the propagation characteristics of thermally and elastically induced waves and shows how photothermal coupling alters material behavior. The profiles elucidate the spatial heterogeneity of the examined variables and illustrate how the different components develop energy and mechanical deformation resistance within the domain. In accordance with the established criteria, the coupled photothermoelastic theory with variable thermal conductivity builds upon the spatial dependence of the physical parameters, denoted as distance x, illustrated in Figures 1–10. The numerical computations correspond to time $t = 0.5$.

Figure 1 shows that the boundary $x = 0$ has the greatest temperature θ, which then rapidly decreases with increasing x and approaches almost 0 away from the source. For the varying thermal conductivities, greater negative values of α mean less temperature magnitude at that position (point in space). Thus, the temperature of all curves at $\alpha = 0$ will always be greater than all other curves (the $\alpha = -3$ case will be the lowest). This is strongest with non-linear/variable conductivity as the temperature is more than the previously stated conditions. The FEA (Finite Element Analysis) results and alpha zero results are in close agreement, showing that the numerical results are valid. Also in Figure 6, for the $\alpha = -2$ non-linear case, temperature decreases with distance. For the heat-flux pulse case (interval) time $t_p = 0.2$ and $t_p = 0.5$, longer pulse times give overall weaker temperature response (lower) than shorter pulse times (higher).

In Figure 2, the displacement u varies strongly near the heated boundary, starting with a negative value at $x = 0$, then increasing rapidly to a small positive peak at a short distance from the surface (around $x \approx 0.3$–0.5), and finally decaying gradually toward zero as x increases, indicating that the thermoelastic deformation is localized near the heating region. The influence of the varying thermal conductivity parameter α is clear: as α becomes more negative, the displacement response is reduced, with both the initial compressive (negative) displacement near $x = 0$ and the subsequent positive peak becoming smaller, while the overall shape (sign change and decay to zero) remains the same; the analytical solution for $\alpha = 0$ agrees well with the FEM curve, supporting the numerical accuracy. In Figure 7, under the nonlinear model, changing the heat-flux pulse time t_p modifies the amplitude of u along the distance: shorter pulse times produce a stronger thermoelastic response (larger magnitude of displacement near the boundary and a higher peak), whereas increasing t_p decreases the displacement magnitude throughout the domain, while preserving the same qualitative behavior of sign change and attenuation with distance.

In Figure 3, the carrier density N rises sharply from the boundary at $x = 0$ to a distinct maximum close to the surface (around $x \approx 1$), and then decreases monotonically with distance, approaching a small value in the far field, which indicates that the excitation generates a localized carrier accumulation near the irradiated region followed by spatial relaxation. The parameter α strongly controls the magnitude of this response: the highest carrier density and largest peak occur for $\alpha = 0$, while making α more negative $(-1, -2, -3)$ progressively lowers N over the whole domain and reduces the peak value, although the general (increase–peak–decay) shape remains unchanged; the analytical solution at $\alpha = 0$ matches the FEM results well, confirming the numerical accuracy. In Figure 8, under the nonlinear model with $\alpha = -2$, varying the heat-flux pulse time t_p modifies the carrier-density amplitude in a similar way: shorter pulse times (e.g., $t_p = 0.2$) produce a stronger carrier-density buildup and a higher peak, whereas increasing t_p (up to 0.5) decreases the peak and lowers N throughout the distance, while preserving the same spatial behavior of near-surface growth followed by decay toward the far-field level.

Figures 4 and 9 show that σ_{xx} is governed by the boundary at $x = 0$, where the heat-flux pulse is applied. Consistent with the mechanical boundary condition at the surface (commonly traction-free, so $\sigma_{xx}(0,t) = 0$), the stress starts from zero at $x = 0$, then quickly becomes compressive and reaches a negative minimum close to the surface ($x \approx 0.4$–0.6), before relaxing and tending to zero as x increases. In Figure 4, the compressive magnitude decreases as α becomes more negative, giving a shallower minimum while preserving the same overall profile; the analytical result for $\alpha = 0$ agrees well with FEM. In Figure 9 (nonlinear model, $\alpha = -2$), increasing the pulse time t_p reduces $|\sigma_{xx}|$ and makes the minimum less pronounced, whereas shorter pulses produce the strongest compressive stress.

Figures 5 and 10 indicate that the electro-chemical potential energy M is boundary-driven: it has its highest value at $x = 0$ (where the heat-flux excitation is applied) and then decreases smoothly and monotonically with distance, approaching zero far from the surface. In Figure

© 2026 NSP
Natural Sciences Publishing Cor.

5, the parameter α mainly affects the magnitude: M is largest for $\alpha = 0$ and progressively decreases as α becomes more negative $(-1, -2, -3)$, while the same exponential-like decay trend is preserved; the analytical solution at $\alpha = 0$ agrees well with FEM. In Figure 10 (nonlinear model with $\alpha = -2$), increasing the heat-flux pulse time t_p reduces M across the domain: shorter pulses yield higher potential energy levels, whereas longer pulses produce a weaker response, with all curves still decaying to zero as x increases.

5 Conclusion

The present work examines a fully coupled GNIII-based semiconductor model incorporating variable (temperature-dependent) thermal conductivity in a half-space. The medium is assumed initially quiescent, with all fields and their time derivatives set to zero and is excited at the boundary $x = 0$ by traction-free and zero-carrier conditions in conjunction with a prescribed pulsed heat flux. To obtain stable and accurate solutions of the resulting coupled nonlinear PDEs, a Galerkin finite element formulation is developed and integrated in time using an implicit scheme, leading to a nonlinear algebraic system that is solved iteratively at each time step. The computed responses (Figures 1–10) show that the temperature, displacement, carrier density, normal stress, and electro-chemical potential energy are concentrated near the loaded surface and decay with distance into the half-space. The variable-conductivity parameter α governs the response amplitude: increasingly negative α values reduce the magnitudes of all field variables while preserving the same qualitative spatial behavior. Under the nonlinear model, increasing the heat-flux pulse time t_p further diminishes the responses throughout the domain, indicating that longer pulses generate a weaker thermo–electro–mechanical disturbance. Finally, the close agreement between the FEM results and the available analytical solution for the reference case $\alpha = 0$ verifies the accuracy of the proposed numerical framework and supports its suitability for analyzing coupled wave phenomena in semiconductors with variable thermal properties.

Acknowledgment

The authors extend their appreciation to Umm Al-Qura University, Saudi Arabia for funding this research work through grant number: 26UQU4380170GSSR01.

Funding

This research work was funded by Umm Al-Qura University, Saudi Arabia under grant number: 26UQU4380170GSSR01.

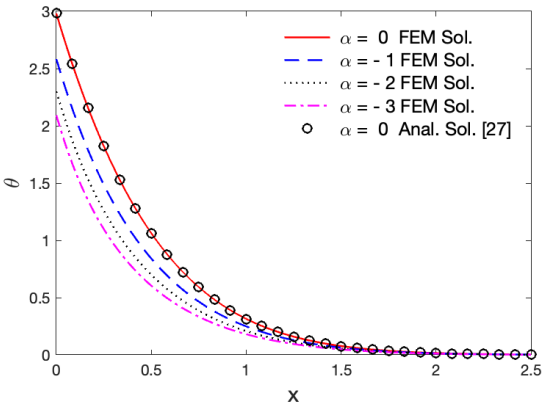


Fig. 1: Temperature variations θ versus x for various values of α.

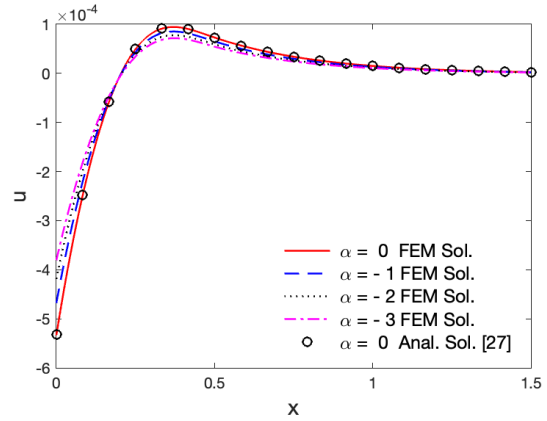


Fig. 2: Displacement variations u versus x for various values of α.

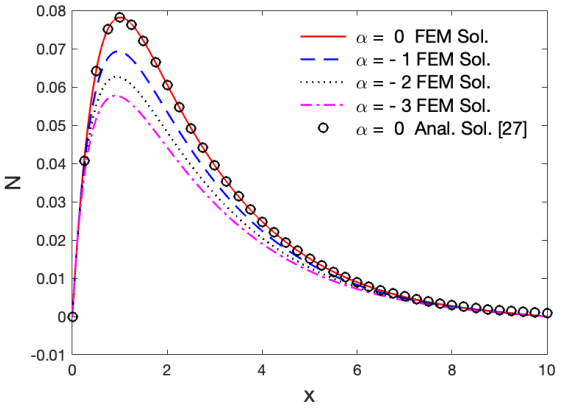


Fig. 3: Carrier density variation N versus x for various values of α.

© 2026 NSP
Natural Sciences Publishing Cor.

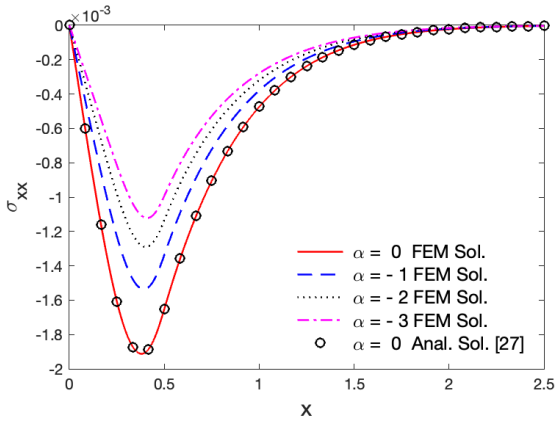


Fig. 4: Stress variations σ_{xx} versus x for various values of α.

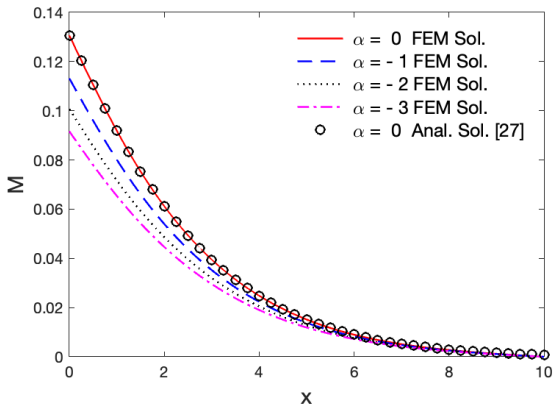


Fig. 5: Electro-chemical potential variation M versus x for various values of α.

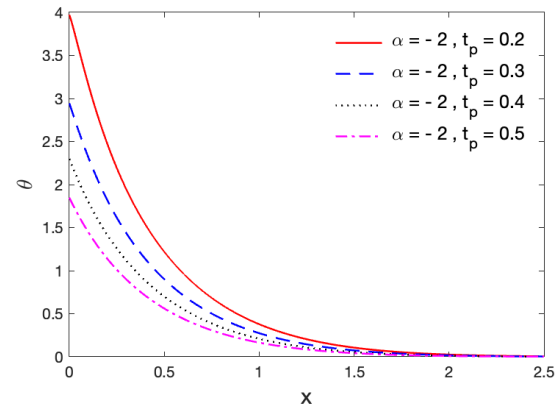


Fig. 6: Temperature variations θ versus x for various values of t_p under the nonlinear model.

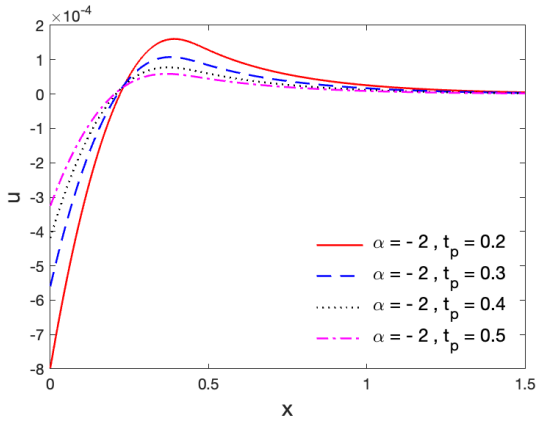


Fig. 7: Displacement variations u versus x for various values of t_p under the nonlinear model.

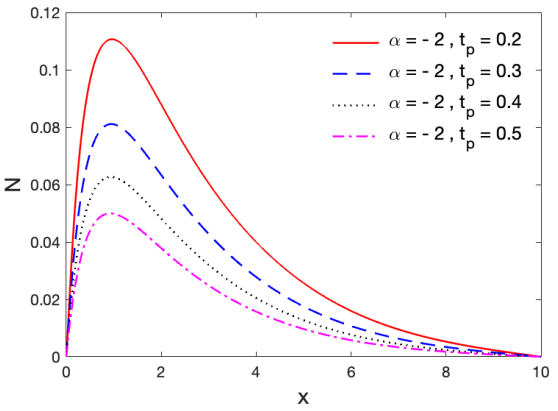


Fig. 8: Carrier density variation N versus x for various values of t_p under the nonlinear model.

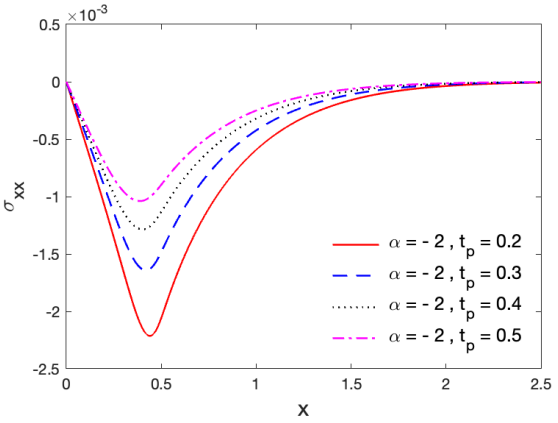


Fig. 9: Stress variations σ_{xx} versus x for various values of t_p under the nonlinear model.

© 2026 NSP
Natural Sciences Publishing Cor.

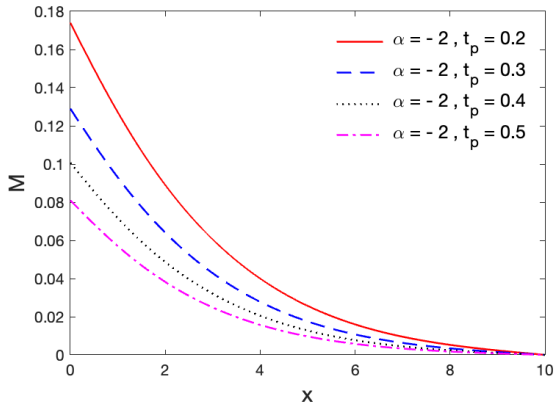


Fig. 10: Electro-chemical potential variation M versus x for various values of t_p under the nonlinear model.

References

[1] Biot, M. A., Thermoelasticity and irreversible thermodynamics. *Journal of Applied Physics*, 1956, 27(3), 240–253.

[2] Cattaneo, C., A form of heat-conduction equations which eliminates the paradox of instantaneous propagation. *Comptes Rendus*, 1958, 247, 431.

[3] Lord, H. W. and Shulman, Y., A generalized dynamical theory of thermoelasticity. *Journal of the Mechanics and Physics of Solids*, 1967, 15(5), 299–309.

[4] Green, A. E. and Lindsay, K. A., Thermoelasticity. *Journal of Elasticity*, 1972, 2(1), 1–7.

[5] Green, A. E. and Naghdi, P. M., Thermoelasticity without energy dissipation. *Journal of Elasticity*, 1993, 31(3), 189–208.

[6] Green, A. E. and Naghdi, P., A re-examination of the basic postulates of thermomechanics. *Proceedings of the Royal Society of London. Series A: Mathematical and Physical Sciences*, 1991, 432(1885), 171–194.

[7] Todorović, D., Photothermal and electronic elastic effects in microelectromechanical structures. *Review of Scientific Instruments*, 2003, 74(1), 578–581.

[8] Todorović, D., Plasma, thermal, and elastic waves in semiconductors. *Review of Scientific Instruments*, 2003, 74(1), 582–585.

[9] Song, Y., et al., Study of photothermal vibrations of semiconductor cantilevers near the resonant frequency. *Journal of Physics D: Applied Physics*, 2008, 41(15), 155106.

[10] Hobiny, A. and Abbas, I., A GN model on photothermal interactions in a two-dimensions semiconductor half space. *Results in Physics*, 2019, 15, 102588.

[11] Abbas, I., Hobiny, A. and Marin, M., Photo-thermal interactions in a semi-conductor material with cylindrical cavities and variable thermal conductivity. *Journal of Taibah University for Science*, 2020, 14(1), 1369–1376.

[12] Alzahrani, F. S. and Abbas, I. A., Photo-thermo-elastic interactions without energy dissipation in a semiconductor half-space. *Results in Physics*, 2019, 15, 102805.

[13] Alzahrani, F., The effects of variable thermal conductivity in semiconductor materials photogenerated by a focused thermal shock. *Mathematics*, 2020, 8(8), 1230.

[14] Ailawalia, P. and Kumar, A., Ramp type heating in a semiconductor medium under photothermal theory. *Silicon*, 2019, 1–10.

[15] Lotfy, K., et al., Response of electromagnetic and Thomson effect of semiconductor medium due to laser pulses and thermal memories during photothermal excitation. *Results in Physics*, 2020, 16, 102877.

[16] Mohamed, M. S., et al., Absorption illumination of a 2D rotator semi-infinite thermoelastic medium using a modified Green and Lindsay model. *Case Studies in Thermal Engineering*, 2021, 26.

[17] Yang, W., et al., Numerical investigations of the effects of different factors on the displacement of energy pile under the thermo-mechanical loads. *Case Studies in Thermal Engineering*, 2020, 21.

[18] Khoukhi, M., Abdelbaqi, S. and Hassan, A., Transient temperature change within a wall embedded insulation with variable thermal conductivity. *Case Studies in Thermal Engineering*, 2020, 20.

[19] Ghasemi, S. E., Hatami, M. and Ganji, D. D., Thermal analysis of convective fin with temperature-dependent thermal conductivity and heat generation. *Case Studies in Thermal Engineering*, 2014, 4, 1–8.

[20] Khamis, A. K., Lotfy, K. and El-Bary, A. A., Effect of variable thermal conductivity of semiconductor elastic medium during photothermal excitation subjected to thermal ramp type. *Waves in Random and Complex Media*, 2020, 32(1), 78–90.

[21] Gupta, V., Barak, M. S. and Das, S., Vibrational analysis of size-dependent thermo-piezo-photo-electric semiconductor medium under memory-dependent Moore–Gibson–Thompson photo-thermoelasticity theory. *Mechanics of Advanced Materials and Structures*, 2023, 31(28), 10543–10559.

[22] Mahrous, S. A., et al., Two-dimensional problem for an infinite body of two coaxial cylinders under the action of a solenoidal body force in the theory of thermoelastic diffusion. *Journal of Thermal Stresses*, 2024, 47(10), 1371–1385.

[23] Gupta, V. and Barak, M. S., Photo-thermo-piezo-elastic waves in semiconductor medium subject to distinct two temperature models with higher order memory dependencies. *International Journal of Numerical Methods for Heat & Fluid Flow*, 2023, 34(1), 84–108.

© 2026 NSP
Natural Sciences Publishing Cor.

[24] Gupta, V. and Barak, M. S., Fractional and MDD analysis of piezo-photo-thermo-elastic waves in semiconductor medium. *Mechanics of Advanced Materials and Structures*, 2023, 31(25), 6787–6802.
[25] Gupta, V., Barak, M. S. and Ahmad, H., Reflection of quasi plasma wave in photo-piezo semiconductor medium with distinct higher order fractional derivative two temperature models. *Physica Scripta*, 2024, 99(2).
[26] Sherief, H., et al., A fully coupled system of generalized thermoelastic theory for semiconductor medium. *Scientific Reports*, 2024, 14(1).
[27] Abbas, I., Almuneef, A. and El-Bary, A. A., A novel photo-thermoelastic wave model in semiconductor media based on GNIII theory. *International Communications in Heat and Mass Transfer*, 2025, 165, 109032.
[28] Lotfy, K., Effect of variable thermal conductivity during the photothermal diffusion process of semiconductor medium. *Silicon*, 2019, 11(4), 1863–1873.
[29] Lotfy, K., et al., Thermomechanical response model on a reflection photothermal diffusion waves (RPTD) for semiconductor medium. *Silicon*, 2019, 1–11.
[30] Abbas, I. A. and Marin, M., Analytical solutions of a two-dimensional generalized thermoelastic diffusions problem due to laser pulse. *Iranian Journal of Science and Technology, Transactions of Mechanical Engineering*, 2018, 42(1), 57–71.
[31] Hobiny, A. and Abbas, I. A., Analytical solutions of photo-thermo-elastic waves in a non-homogenous semiconducting material. *Results in Physics*, 2018, 10, 385–390.
[32] Abbas, I. A., Alzahrani, F. S. and Elaiw, A., A DPL model of photothermal interaction in a semiconductor material. *Waves in Random and Complex Media*, 2019, 29(2), 328–343.
[33] Abbas, I. A., Eigenvalue approach on fractional order theory of thermoelastic diffusion problem for an infinite elastic medium with a spherical cavity. *Applied Mathematical Modelling*, 2015, 39(20), 6196–6206.
[34] Zhang, Q., Sun, Y. and Yang, J., Thermoelastic responses of biological tissue under thermal shock based on three phase lag model. *Case Studies in Thermal Engineering*, 2021, 28.
[35] Abbas, I. and Hobiny, A. D., Analytical-numerical solutions of photo-thermal interactions in semiconductor materials. *Information Sciences Letters*, 2021, 10(2), 189–196.
[36] Selim, M. M., Effect of thermal stress and magnetic field on propagation of transverse wave in an anisotropic incompressible dissipative initially stressed plate. *Applied Mathematics & Information Sciences*, 2017, 11(1), 195–200.
[37] Bassiouny, E., Mathematical model for hyperbolic two temperature fractional-order thermoelastic materials subjected to thermal loading. *Applied Mathematics and Information Sciences*, 2021, 15(1), 23–29.
[38] Zaim, A., et al., Galerkin finite element analysis of magneto-hydrodynamic natural convection of Cu-water nanoliquid in a baffled U-shaped enclosure. *Propulsion and Power Research*, 2020, 9(4), 383–393.
[39] Marzougui, S., et al., Entropy generation and heat transport of Cu–water nanoliquid in porous lid-driven cavity through magnetic field. *International Journal of Numerical Methods for Heat & Fluid Flow*, 2021, 32(6), 2047–2069.
[40] Pushpa, B. V., Sankar, M. and Mebarek-Oudina, F., Buoyant convective flow and heat dissipation of Cu–H_2O nanoliquids in an annulus through a thin baffle. *Journal of Nanofluids*, 2021, 10(2), 292–304.
[41] Rajashekhar, C., et al., Mass and heat transport impact on the peristaltic flow of a Ree–Eyring liquid through variable properties for hemodynamic flow. *Heat Transfer*, 2021, 50(5), 5106–5122.
[42] Abouelregal, A. E., Marin, M. and Öchsner, A., A modified spatiotemporal nonlocal thermoelasticity theory with higher-order phase delays for a viscoelastic micropolar medium exposed to short-pulse laser excitation. *Continuum Mechanics and Thermodynamics*, 2024, 37(1), 15.
[43] Marin, M. and Öchsner, A., *Essentials of Partial Differential Equations*. Springer, Cham, Switzerland, 2018.
[44] Marin, M. and Öchsner, A., The effect of a dipolar structure on the Hölder stability in Green–Naghdi thermoelasticity. *Continuum Mechanics and Thermodynamics*, 2017, 29(6), 1365–1374.
[45] Abbas, I., et al., Analysis of thermoelastic interaction in a polymeric orthotropic medium using the finite element method. *Polymers*, 2022, 14(10), 2112.
[46] Abbas, I., et al., Generalized thermoelastic interaction in a half-space under a nonlocal thermoelastic model. *Mathematics*, 2022, 10(13).
[47] Marin, M., Harmonic vibrations in thermoelasticity of microstretch materials. *Journal of Vibration and Acoustics*, 2010, 132(4), 0445011–0445016.
[48] Vlase, S., et al., Energy of accelerations used to obtain the motion equations of a three-dimensional finite element. *Symmetry*, 2020, 12(2).
[49] Abouelregal, A. E., Marin, M. and Öchsner, A., The influence of a non-local Moore–Gibson–Thompson heat transfer model on an underlying thermoelastic material under the model of memory-dependent derivatives. *Continuum Mechanics and Thermodynamics*, 2023, 35(2), 545–562.
[50] Abbas, I., et al., A study on a novel photothermal without energy dissipation model in semiconductor materials. *Mechanics of Solids*, 2025, 60(4), 2617–2630.
[51] Sherief, H., et al., The effect of the surface recombination velocity on 2D thermoelastic semiconductor solid sphere problem. *Alexandria*

© 2026 NSP
Natural Sciences Publishing Cor.

Engineering Journal, 2025, 127, 1126–1142.
[52] Sherief, H. H. and Hamza, F. A., Modeling of variable thermal conductivity in a generalized thermoelastic infinitely long hollow cylinder. *Meccanica*, 2015, 51(3), 551–558.
[53] Abbas, I. A. and Kumar, R., Deformation due to thermal source in micropolar generalized thermoelastic half-space by finite element method. *Journal of Computational and Theoretical Nanoscience*, 2014, 11(1), 185–190.
[54] Mohamed, R., Abbas, I. A. and Abo-Dahab, S., Finite element analysis of hydromagnetic flow and heat transfer of a heat generation fluid over a surface embedded in a non-Darcian porous medium in the presence of chemical reaction. *Communications in Nonlinear Science and Numerical Simulation*, 2009, 14(4), 1385–1395.
[55] Yoon, H. C., Vasudeva, K. K. and Mallikarjunaiah, S. M., Finite element model for a coupled thermo-mechanical system in nonlinear strain-limiting thermoelastic body. *Communications in Nonlinear Science and Numerical Simulation*, 2022, 108, 106262.
[56] Shekhar, S., Comparative study of thermal effect on thermoelastic double porous solid by finite element method and finite-infinite element method. *Waves in Random and Complex Media*, 2023, 1–22.
[57] Xu, Z., Guo, H. and Shang, F., A nonlinear non-Fourier thermoelasticity model with high-order temperature-dependent material properties and time-domain finite element method to impact responses of 2D metallic solids under ultra-short pulsed laser heating. *International Journal of Applied Mechanics*.
[58] Alsaqoor, S., et al., Higher-order finite element implementation of non-axisymmetric thermoelastic analysis in long functionally graded material hollow cylinder. *Advances in Science and Technology Research Journal*.
[59] Saeed, T., Hybrid finite element method to thermo-elastic interactions in a piezo-thermo-elastic medium under a fractional time derivative model. *Mathematics*, 2022, 10(4), 650.
[60] Song, Y., et al., Bending of semiconducting cantilevers under photothermal excitation. *International Journal of Thermophysics*, 2014, 35(2), 305–319.

© 2026 NSP
Natural Sciences Publishing Cor.